VALIDATION OF CFD FOR THE FLOW AROUND A COMPUTER SIMULATED PERSON IN A MIXING VENTILATED ROOM

Chris N. Sideroff and Thong Q. Dang
STAR Center for Environmental Quality Systems
Syracuse University, Syracuse, New York, USA

ABSTRACT

This paper gives a summary of a detailed Computational Fluid Dynamics (CFD) study of the flow around a Computer Simulated Person (CSP) for the purpose of validation. This was conducted using a canonical building environment scenario of the mixing ventilation type and included verification against test data. The contribution of this work was identifying the necessary requirements of several computational aspects such as grid resolution, boundary conditions and turbulence models that are needed for the accurate CFD simulation of the Personal Micro-Environment (PME), i.e. the person's breathing zone.

1. INTRODUCTION

CFD has been used with success in a variety of areas in the indoor environment community. An important area of interest is the interaction of humans with their PME, an area that draws considerable attention due to its relation to indoor air quality (Murakami 2004, Sørensen and Voigt 2003, Bjørn and Nielsen 2002). CFD has augmented the abilities of researchers in this field because of its flexibility to model a wide range of problems quickly at potentially lower costs.

To be able to use CFD as a design tool, one first must have confidence that it can predict the desired flow with a certain degree of accuracy. To do this two important questions need to be answered. First, is CFD capable of predicting the flow in question and second, what is needed to do so? To answer these questions, standard or canonical benchmark cases are needed so the individual issues may be identified while providing a consistent approach for others researchers to use.

The collaborative efforts of P.V. Nielsen, S. Murakami, S. Kato, C. Topp and J-H. Yang have culminated in a benchmark test for evaluating CFD in the personal micro-environment (Nielsen et al., 2003). They have proposed two canonical building environment scenarios: mixing and displacement ventilated rooms with a centrally situated CSP. Only the mixing ventilation setup was studied here. The primary objective of this study was, using a benchmark case, to identify the key requirements needed to achieve an accurate prediction of the detailed flow field around a CSP.

2. MIXING VENTILATION SETUP

A summary of the geometry setup, boundary conditions and reporting method of the benchmark test cases are outlined in Nielsen et al. (2003). Figure 1 provides a detailed schematic of the mixing ventilated room used for both the experiment and simulations. CFD results were extracted and compared at the same locations the experimental data was measured. The dimensions and measurements locations of the mixing ventilated room are again found in Nielsen et al. (2003). The CSP geometry model was obtained from Kato's research group at the University of Tokyo, who created the digitization of a female mannequin using a stereo-lithographic technique.

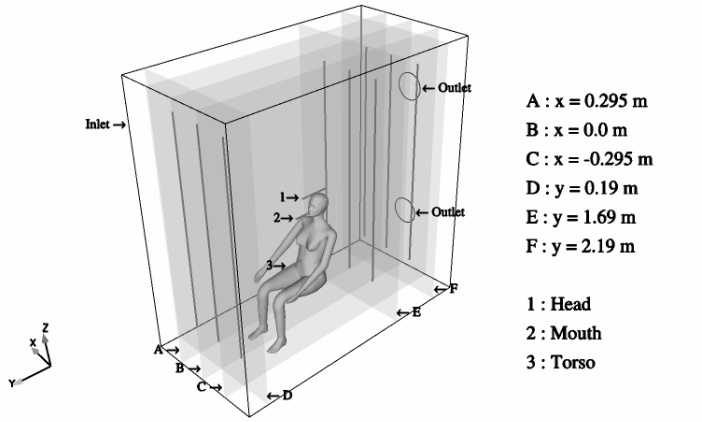

Figure 1. *Mixing Ventilated Room Configuration - Measurement Locations*

3. COMPUTATIONAL ASPECTS

The commercial CFD software FLUENT (v. 6.2) was used for this work and the following outlines the numerical models selected for use in FLUENT. The numerical convective scheme used for all the transport equations was a 2nd order accurate upwind scheme. Pressure-velocity coupling was handled by the SIMPLEC algorithm combined with the second-order pressure interpolation. Reynolds Averaged Navier-Stokes (RANS) turbulence modeling was exclusively used in this work. A Beowulf cluster with 64 1.6 GHz processors (x86-64 architecture) and 64 Gbytes of total system memory made this type of analysis possible. Twelve processors were typically used, which took anywhere from 12 to 48 hours depending on the grid resolution and turbulence model used.

Convergence of transport equation residuals was monitored and typically dropped 4 orders of magnitude for the continuity residual (two to three orders lower for other equations). The number of iterations required to reach convergence varied but was typically several thousand. It was noted that average residuals alone were not always a good indication of convergence. In particular, for the v^2-f calculations other values, such as velocity magnitude, were monitored at strategically chosen points to give a better indication that the solution had indeed converged.

4. GRID DEPENDENCY

Due to the unknown behavior of the global and local flow features around the CSP, selecting the appropriate grid was non-trivial. The initial grid, Grid A, had 25x50x50 nodes along the *x, y, z* edges, respectively, of the walls and 9000 nodes on the CSP surface resulting a volume grid of 1.2×10^6 tetrahedral cells. A second, Grid B, was made up of 37x75x75 nodes along the *x, y, z* edges, respectively, of the walls and 18,000 nodes on the CSP surface resulting in 2.0×10^6 tetrahedral cells. To establish a grid independent solution a third grid, Grid C, was constructed, in a similar manner to Grids A and B, which contained 3.3×10^6 tetrahedral cells. For the grid dependency simulations a uniform inlet velocity profile along with the standard k-ε turbulence model was used.

Streamlines, shown in Fig. 2(a), around the shoulder and neck region indicate the behavior of the solutions from each grid. The flow patterns of Grid B and C are nearly the same while the flow pattern of Grid A is not. The coarseness of Grid A caused a larger percentage of the flow originating from the shoulder and neck to leave through the upper outlet hole, whilst the majority of this flow in the other two solutions leaves through the bottom hole. This is clearly seen in Fig. 2(b) where the velocity profile located slightly downstream of the CSP in the mid-plane (see St. E, Fig. 1) from Grid A has a much larger deficit than either Grid B or C.

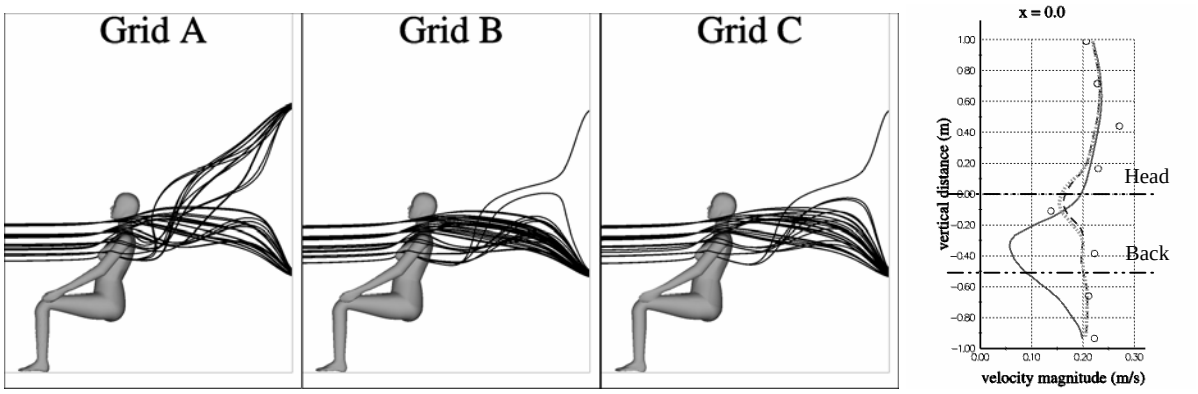

(a) *(b)*

Figure 2. *(a) Streamlines (b) Velocity Profiles:*
o *, exp. data;* ——— *, Grid A;* – – – *, Grid B;* ····· *, Grid C*

While the simulations with Grids B and C provided a better prediction of the flow away from the CSP, this was not true near the CSP. In particular, the CFD results with these 3 grids did not compare well against test data at the three additional locations near the head, mouth and torso. The near-wall results are discussed further in Sec. 6.

5. BOUNDARY CONDITIONS

All values at the inlet boundary were initially assumed uniform (“plug flow") and are summarized in Nielsen et al. (2003). However, the velocities measured at the inlet were found not to be uniform, rendering the assumption for the computation inaccurate. There were no experimental measurements taken at the inlet but velocity magnitude was measured slightly (y = 0.19 m) downstream of the inlet. At this location, the difference between the CFD with a uniform inlet velocity and experiment was as large as 100%, as seen in Fig. 3(a). Upon examining the solution at other locations, it was observed that the error at the inlet propagated downstream but decreased in magnitude.

A reconstruction of the inlet boundary profile was made using the existing experimental data. Note that since the inflow velocity profile was not symmetric across the y-z plane located at x = 0, the full computational domain was required (see Fig. 1). A 2D bi-cubic interpolation algorithm was employed to perform the interior reconstruction, and a polynomial profile was chosen to extrapolate the inner data to the walls. The polynomial order was estimated to be 2 by using an iterative procedure until the mass-flow was equal to that of the uniform case. CFD results on Grid B using the reconstructed inlet profile are shown as the dashed lines in Fig. 3(a). Figure 3(b) shows comparisons of the velocity profiles downstream of the CSP, showing improvements in the CFD results with the non-uniform inlet velocity profile correction. However, the CFD results again did not compare well against test data near the head, mouth and torso locations.

No information was provided in the benchmark study at the two outlet holes. Consequently, a sensitivity study was carried out at the outflow boundaries using three different boundary conditions. The first two used were outflow and pressure outlet boundary conditions and the third included the actual duct leaving the outlet holes. Virtually no variations were seen between the velocity magnitude profiles of each at any measurement locations. In addition, for each case, the mass-flow through the top and bottom holes was calculated and compared. Again, all three cases provided nearly identical values: both predicting 50% of the flow through each hole. While careful examination of all scenarios indicated little difference, due to the pressure outlet condition’s ability to handle reversed flow

it provided more stability during convergence of the solution. All subsequent calculations were run using the pressure outlet boundary condition.

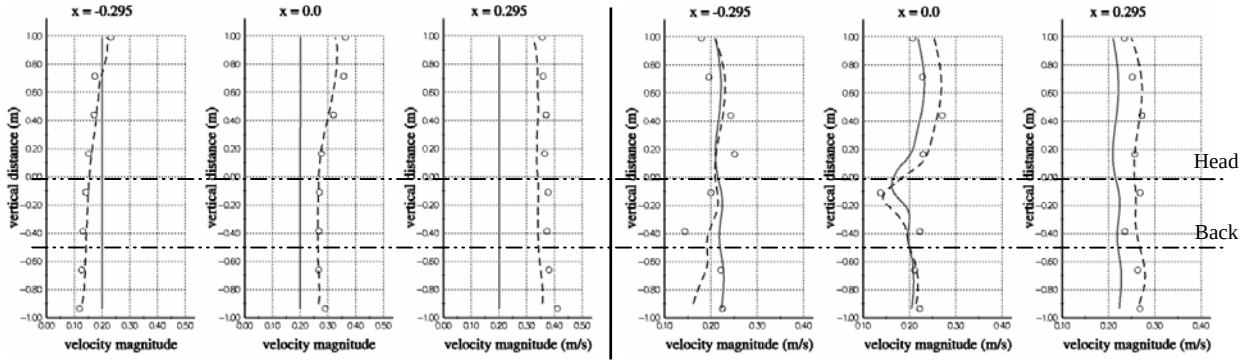

(a) y = 0.19 m *(b) y = 1.69 m*

Figure 3. *Velocity Magnitude, Grid B:*
o *, exp. data;* ——— *, Uniform Inlet;* – – *, Non-Uniform Inlet*

To simulate the heat transfer of human skin, Nielsen et al. (2003) includes values for the radiative and convective heat transfer. Values of 38 *W* for both correspond to the activity level of a seated relaxed person. To simplify the investigation, no radiative heat transfer was included and only the convective part was used for the CSP thermal boundary condition. Along with the heat flux, a zero tangential velocity (no-slip) was enforced on the CSP surface. Zero heat flux and no-slip conditions were applied to all other walls.

6. TURBULENCE MODELS

While the impact of the grid resolution and boundary conditions were understood there was still significant error in the predictions near the CSP. Predictions at the mouth, head and torso using the standard k-ε on any grid did not compare well. As a consequence, two other RANS turbulence models available in FLUENT were investigated: the Abe-Kondoh-Nagano (AKN) low-*Re* k-ε and v^2-f models.

It is well known that the standard k-ε model over-predicts the production of turbulent kinetic energy near solid walls. Low-*Re* k-ε models introduce damping functions which attempt to correct the near wall behavior. These damping functions allow integration through the entire boundary layer without the direct use of wall functions and as a result generally require much finer grids than the standard k-ε. Typically y^+ [1] needs to be on the order of 1 and optimally less than 1. As such, the low-*Re* k-ε model was only used with Grids B and C. Full details of the AKN low-*Re* k-ε model are found in Abe et al. (1994). However, the low Reynolds number corrections could not conceal the inherent deficiencies of the two-equation k-ε model (currently implemented in FLUENT v. 6.2).

A recent turbulence model dubbed the v^2-f, possessing the ability to model some anisotropic turbulence effects, was also included this work. The v^2-f model, originally proposed by Durbin (1991), employs nearly identical forms of the k and ε equations while including two new ones: the first, a transport equation for the wall normal Reynolds stress, v^2,

[1] Where $y^+ = \frac{y_p u^*}{\nu} : y_p$ is the distance from wall adjacent cell-center to the wall, the friction velocity $u^* = \sqrt{\frac{\tau_{wall}}{\rho}}$ and ν is the kinmatic viscosity

and the second, an elliptic equation modeling the non-local effects of the fluctuating pressure-rate-of-strain correlation, *f*. The most conspicuous change invoked by the v^2-*f* model, as compared to the k-ε approach, is in the definition of the eddy viscosity, $\nu_T = C_\mu (v^2)^{1/2} \tau$, which instead uses $(v^2)^{1/2}$ as the velocity scale and a time scale that can account for realizibility. The reader is redirected to Sveningsson (2003) for further details. Similar to the low-*Re* k-ε, the v^2-*f* integrates the flow all the way through the boundary layer, and as such requires y^+ on the order of or less than 1. In contrast to the low-*Re* k-ε, however, the v^2-*f* does not use an ad-hoc function, but instead models the near-wall behavior through a more physical approach: the v^2 and *f* equations.

Figure 5 shows a comparison of three quantities for each turbulence model at the mouth. The left plot of Fig. 5 compare the vertical velocity (*z* component) along with the experimental data (circle symbols). Overall the v^2-*f* predicts the trend and magnitude better than the other two; however very near the CSP the error increases (error in data unknown). More interesting results are observed in the turbulence intensity, defined as $I = \sqrt{\frac{2}{3}k}\,/U_{inlet}$, and temperature profiles. The importance of mean velocity, air temperature and turbulence intensity on the percentage of people dissatisfied (PD) has been well studied - Fanger et al. (1988) even developed an empirical equation relating these parameters. A plot of turbulence intensity (top right in Fig. 5) near the mouth revealed a maximum difference of 17% among the models, while a 4 K variation was observed in surface temperature (bottom right in Fig. 5). The results for turbulence intensity or temperature could not be verified because Nielsen et al. (2003) does not include this data; however, they have important consequences when assessing thermal comfort.

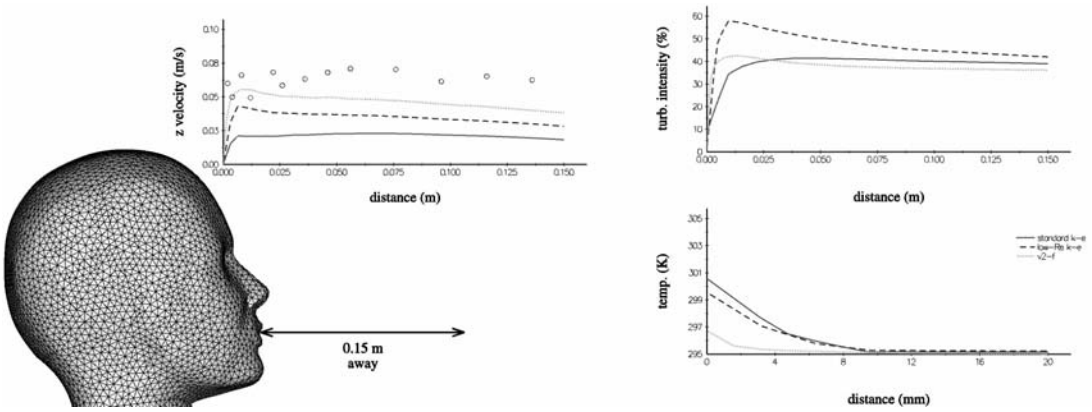

Figure 5. *Profiles near CSP Mouth, Grid C:*
——, standard k-ε; – – , low-Re k-ε; ····· , v^2-f

7. CONCLUSIONS AND FUTURE CONSIDERATIONS

The objective of this study was to evaluate the applicability of CFD for the personal micro-environment. Specifically, two important questions needed to be answered: Was CFD able to predict these flows and what requirements were necessary? Although, no other CFD results using the benchmark case of Nielsen et al. (2003) have yet been published, this work illustrated CFD can predict PME flows with confidence. To achieve this it was found several key issues needed to be addressed.

To achieve grid convergence, at the very least, with tetrahedral cells a few million were needed. Consideration of the number of grid cells not only near the CSP but also in regions of unknown flow behavior was required. For example, the wake behind CSP head was found to be one these regions. While resolving the far field may weakly influence, say, the thermal

comfort, it quite possibly could have a dramatic impact on pollutant and particulate exposure (Sideroff and Dang 2005). Using tetrahedral cells for the entire domain simplifies grid generation for complex geometries but require considerably more cells to resolve the boundary layer. By including several layers of prismatic cells on the CSP surface and using tetrahedral cells elsewhere, the boundary layer was resolved with little added expense.

Accurate quantification of boundary conditions is also important. For this case, although test case suggests uniform inlet conditions, analysis of the experimental data near the inlet uncovered a large spatial non-uniformity, rendering the initial “plug flow" assumption inaccurate. A non-uniform inlet boundary condition was constructed that lead to a significant improvement in the predictions. Outflow and pressure outlet boundary conditions along with the actual duct geometry were evaluated yielding little differences between solutions. The pressure outlet condition was chosen for all subsequent calculations owing to its simplicity and enhanced convergence stability.

The standard k-ε along with the AKN form of the low-*Re* k-ε model and Durbin’s recent v^2-f model were examined. The CFD results showed that the v^2-f better predicted the flow near the CSP. Turbulence intensity and temperature profiles near the CSP illustrated large differences between the three models. The variations of these parameters affect the estimation of PD. Although no experimental data was available for turbulence intensity or temperature to verify the results, the point of resolving the near-wall flow was made.

ACKNOWLEDGMENTS

This work was supported by the US Environmental Protection Agency (EPA) through the STAR Center for Environmental Quality Systems (www.eqstar.org) and the Center of Excellence in Environmental Systems (www.CoEES.org) at Syracuse University.

REFERENCES

Abe, K., Kondoh, T., and Nagano, Y. 1994 “A New Turbulence Model for Predicting Fluid Flow and Heat Transfer in Separating and Reattaching Flows - I. Flow Field Calculations" *International Journal of Heat and Mass Transfer* Vol. 37, No. 1, pp. 139-151

Bjørn, E. and Nielsen, P.V. 2002 “Dispersal of Exhaled Air and Personal Exposure in Displacement Ventilated Rooms" *Indoor Air* Vol. 12, No. 2, pp. 147-164

Durbin, P.A. 1991 “Near-Wall Turbulence Closure Modeling without ‘Damping Functions’" *Theoretical and Computational Fluid Dynamics* Vol. 3, pp. 1-13

Fanger, P.O., Melikov, A.K., Hanzawa, H. and Ring, J. 1998 “Air Turbulence and Sensation of Draught" *Energy and Buildings* Vol. 12, pp. 21-39

Murakami, S. 2004 “Analysis and Design of the Micro-Climate around the Human Body with Respiration with CFD” *Indoor Air* Vol. 14, Suppl. 7, pp. 144-156

Nielsen, P.V., Murakami, S., Kato, S., Topp, C. Yang, J-H. 2003 “Benchmarks Test for a Computer Simulated Person" *Aalborg University, Indoor Environmental Engineering*

Sideroff, C.N. and Dang, T.Q. 2005 “CFD Analysis of the Flow around a Computer Simulated Person in a Displacement Ventilated Room” *Conference Proceedings, Indoor Air 2005,* Beijing, China

Søresen, D.N. and Voigt L.K. 2003 “Modelling Flow and Heat Transfer around a Seated Human Body by Computational Fluid Dynamics", *Building and Environment* Vol. 38, pp. 753-762

Sveningsson, A. 2003 “Analysis of the Performance of Different v^2-f Turbulence Models in a Stator Vane Passage Flow", *Ph.D Thesis,* Chalmers University of Technology